Journal of Building Engineering 46 (2022) 103730

Contents lists available at ScienceDirect

Journal of Building Engineering

journal homepage: www.elsevier.com/locate/jobe

Shear strength assessment of reinforced concrete components containing EAF steel slag aggregates

Amaia Santamaría [a], Jesús María Romera [a], Ignacio Marcos [a], Víctor Revilla-Cuesta [b], Vanesa Ortega-López [b,*]

[a] Department of Mechanical Engineering, University of the Basque Country, UPV/EHU, Escuela de Ingeniería de Bilbao, I (bloque B) - UPV/EHU, Plaza Ingeniero Torres Quevedo, 1, 48013, Bilbao, Spain
[b] Department of Civil Engineering, University of Burgos, Escuela Politécnica Superior, Calle Villadiego s/n, 09001, Burgos, Spain

ARTICLE INFO

Keywords:
Electric arc furnace slag
Sustainable binder
Fiber-reinforced mixes
Self-compacting concrete
Shear strength tests
Strut-tie model

ABSTRACT

Electric Arc Furnace (EAF) slag can be reused as aggregate in Portland cement concrete mixes. The addition of EAFS and other waste co-products (fly ash, blast furnace slag) will modify the binding properties and will, importantly, enhance the global sustainability of such concretes. These mix designs offer acceptable pumpability and self-compaction in the fresh state and can be reinforced with fibers. In this study, eight different concrete mixes are designed within the range of medium-strength concretes (30–50 MPa) and are characterized in both the fresh and the hardened state. Large concrete volumes are used to pour reinforced beams, which are then subjected to small-span high-load tests to evaluate their resistance to shear stress, by analyzing two types of transversal (shear) reinforcement. The tests yielded promising results, contributing additional evidence on the viability of using recycled EAFS aggregate in structural applications. The mechanical behavior of these concretes was closely correlated with the strength predictions calculated with the formulas listed in various international standards.

1. Introduction

The concept of sustainability is partly a response to industrial activity and its environmental consequences, *i.e.* present-day development must not condition the capability of subsequent generations to respond to their own needs on the planet. The concept of the circular economy has become a *leitmotiv* when planning the guidelines for global activity that extends to all types of waste co-products generated in heavy industry and surplus raw materials from manufacturing processes. In consequence, many scientific and technical papers have, over the past few years, addressed the re-use of a wide range of residual materials, in a research area that is today actively promoted and encouraged.

The high volumes of natural resources used in construction and civil engineering convert them into productive sources of waste co-products. Natural resources can be substituted, often advantageously, by waste and co-products. The task of the construction engineer is to do so in an efficient, safe, and ecologically balanced manner [1,2]. The list of waste co-products which can be used in construction and civil engineering is extensive; however the list of by-products that are used in substitution of natural aggregates is much shorter: construction and demolition waste, bottom ash, fly ash, and iron and steel slags [3–12], among others.

* Corresponding author. Civil Engineering Department, EPS University of Burgos, Calle Villadiego s/n, 09001, Burgos, Spain.
E-mail addresses: amaia.santamaria@ehu.es (A. Santamaría), jesusmaria.romera@ehu.eus (J.M. Romera), ignacio.marcos@ehu.eus (I. Marcos), vrevilla@ubu.es (V. Revilla-Cuesta), vortega@ubu.es (V. Ortega-López).

https://doi.org/10.1016/j.jobe.2021.103730
Received 9 October 2020; Received in revised form 3 December 2020; Accepted 20 November 2021
Available online 23 November 2021

EAF slag is generated during the steel production process, following the smelting and refinement of scrap iron, a siderurgic production process that is widespread in northern Spain. The resultant by-product, Electric Arc Furnace Slag (EAFS, acid slag, oxidizing slag, black slag) consists of dark grey to black mineral pebbles, the main characteristics of which are their hardness, toughness, abrasion resistance, chemical stability, and good durability. The useful properties of EAFS have been demonstrated throughout the construction industry [13–25] despite their drawbacks such as lack of stability and high density. Another abundant by-product of steelmaking activity, Ladle Furnace Slag (LFS), has also been analyzed in reference to various applications [26–29] by the authors of this paper among several others.

In this study, EAFS is assessed for its use as a massive aggregate, along with by-products that act as alternative binders (SCM, supplementary cementitious materials) in the presence of Portland clinker, for the manufacture of medium strength load-bearing Reinforced Concrete (RC) components [30–32].

1.1. Significance and scope of the study

At this point in time, research in the field of reinforced concrete that employs large amounts of EAFS aggregate is scarce. The present study continues to develop the work presented in a recent publication [33], in which the authors analyzed medium-strength concrete made with EAFS as the main aggregate and its flexural deformation and delayed failure under sustained loading. It also presented a comparison of the results with the specifications in current standards. Work that is developed here with fresh tests on the mixtures described in the latter article, using a similar typology of beam. A few results that appear in the following sections have already been presented in the aforementioned article [33].

A brief review of steelmaking slags and their use as aggregate in RC must mention the authors from the Korean University of Kongju (Sang-Woo, Yong-Jun, Kil-Hee and others), who pioneered the first studies on the behavior of RC beams manufactured with EAFS aggregate [34–37]. They analyzed the flexural strength of several RC beams, observing comparable behaviors for EAF concrete and ordinary concrete. Their research was completed with a study of the bonding behavior of ribbed reinforcement bars [38], which reported enhanced bonding behavior, due to the presence of EAFS aggregate in the concrete samples.

At around the same time, a team from the University of Padua (Italy) formed of Pellegrino, Faleschini and others [39,40] studied the flexural and shear failure of EAFS-RC beams and other structural features, showing that the ultimate flexural and shear strength was higher in beams containing EAFS concrete compared with those containing natural aggregate concrete. Faleschini et al. [41] also presented similar results to Ref. [38] when using the pull-out test to study the local bonding strength between reinforcement bars and EAF slag concrete.

In this study, several types of medium-strength concretes containing EAFS aggregate are employed as self-compacting, pumpable, and fiber-reinforced concrete [42–44]. They are examined as bearing elements that support shear loading. In the following sections, the components, mix preparation, their mechanical characterization, and the preparation of the beams will all be described. Their description will in some cases be brief, as relevant information may be found in the aforementioned article [33]. However, new data on additional binder types, including active hydraulic additions -fly ash, Ground Granulated Blast Furnace Slag (GGBS), LFS and fibers-will be detailed.

EAFS concrete beams with lengths of 4400 mm, weighing ±0.7 Tons, containing ribbed steel reinforcement bars laid out in longitudinal and transversal directions were prepared and tested to measure their deformation and failure. The results of the shear strength and effort tests [43,45–53] will be detailed in the following sections, as well as some comparisons between our experimental results and the specifications of the ACI, and other European and Spanish standards.

2. Materials and proportions

2.1. Cement

Four types of cement were tested: firstly, a Portland cement type I 52.5 R; secondly, a Portland cement type IV/B–V 32.5-N containing 50% fly ash; thirdly, a Portland cement type II/B–S 42.5-N containing 30% Ground Granulated Blast Furnace Slag (GGBS), and finally a Portland cement type III/B 32.5-N containing 70% GGBS, as per the EN 197-1 standard [54]. Except for the type I 52.5-R cement, all the other binders consisted of Portland clinker mixed with active additions as fly ash (*fa*-V), and *GGBS*, from industrial by-products, as the intention is to enhance general sustainability. A small fraction (6% of the total binder) of LFS [27] was also added to the IIIP mix as an additional active component of Portland cement.

2.2. Admixture, water, natural aggregates and EAF slag

The admixture, provided by CHRYSO®™, (a plasticizer and a viscosity conditioner) consisted of a carboxylate-based water emulsion, the compatibility of which with the EAFS aggregate was highly satisfactory, greatly assisting the preparation of the self-compacting mixes. Mix water from the urban mains supply of the city of Burgos, Spain was used, which contained no compounds with adverse effects on hydraulic mixes.

The fine fraction (passing sieve N° 16, 1.18 mm mesh [55]) consisted of a commercial natural limestone (calcite fraction >95%) with a fineness modulus of 1.5 units, specific gravity 2.65 Mg/m^3. As detailed in previous publications [27,56] by the authors, this limestone fine fraction is added to improve concrete workability up until the consistency required by self-compacting mixtures, to prevent segregation and to compensate for the spontaneous lack of fine particles in the smaller size fraction (0–4) of EAFS.

Electric Arc Furnace slag (EAFS) in two size fractions (fine <4 mm, medium 4–12 mm), supplied by the company Hormor-Zestoa, was crushed and left outdoors for three months of spontaneous weathering. Their fineness moduli were 3.9 and 5.7 units for the fine fraction and for the medium fraction, respectively. Full details on this material may be found in previous publications by the authors

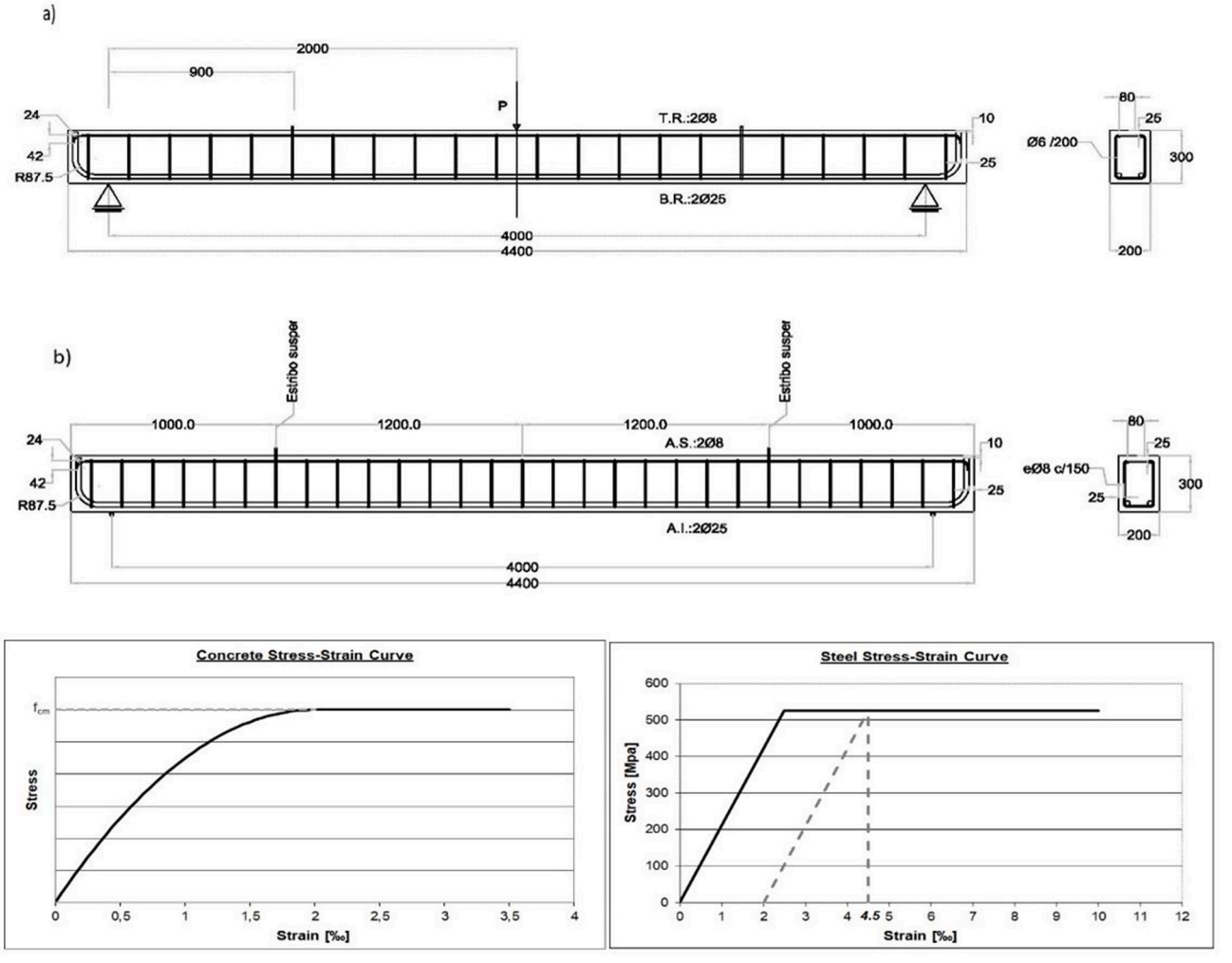

Fig. 1. Beam reinforcement details: a) Types I and IV (Batch 1); b) Types II and III (Batch 2); c) stress-strain curves of materials.

[27,33].

2.3. Rebars and fibers

Two diameters (Ø25mm, Ø8mm) of ribbed steel rebars were used as longitudinal tensile and compressive reinforcements within the beams, together with two diameters (Ø8 mm and Ø6 mm) of transversal shear reinforcement stirrups. The ribbed steel rebars were manufactured from B 500 S steel, in accordance with the specifications of the UNE 36068 standard [57]. The following data may be mentioned: a yield strength of 525 MPa at a theoretical strain of 4.5 thousandths (2 + 525/210 th.) and a horizontal plastic field of up to ten thousandths (Fig. 1c).

Both metallic and synthetic fiber types were separately used in three different mixes of EAFS concrete to assess their efficiency at interacting with the surrounding cementitious matrix [58]. The steel fibers were hook-end wire pieces type HE-55/35 with a length of 35 mm, a diameter of 0.55 mm, a tensile strength of 1200 MPa and a density of 7900 kg/m^3. The polypropylene type T-35 fibers were surface-dimpled pieces with a length of 35 mm, a diameter of 0.93 mm, a tensile strength of 400 MPa, an elastic modulus of 6 GPa, and a density of 910 kg/m^3.

2.4. Mix design and in-fresh characteristics

Eight different concrete mixes were designed for the experimental tests. All the mixes contained the highest possible amounts of EAFS and SCM to satisfy the specifications of a medium strength concrete for use in construction. Three of the mixes were "pumpable" concretes (mixes for on-site pumping) and the other (five) mixes were self-compacting mixes.

As shown in Table 1, the mixes were divided into two batches. Batch 1 refers to four mixes (cast in 2017), detailed descriptions of which may, once again, be found in a previous study [33]; the mixes consisted of cement types I and IV, only some of which had the flowability and the workability for use as self-compacting mixes, unlike the others.

Batch 2 that included four mixes cast in 2018 differed from batch 1 in so far as its mixes incorporated Portland cement types III and II and GGBS. Metallic (M) or Synthetic (S) reinforcing fibers were added to three of the mixes; the IISC mix with no fibers acted as a reference mix, for comparison with the other mixes from batch 2 that included fibers.

The cement amounts (±320–330 kg/m^3) and the w/c ratios (±0.5 units) are standard for medium-strength structural concrete mixtures, forming an acceptable compressive strength (30–50 MPa at 28 days in a moist room). The designed workability of both the pumpable mixes and the self-compacting mixes were a target slump of 200 mm and a target spread on a flat plate of 600 mm within 5 s (both tests using the Abrams cone), respectively. The mix proportioning is shown in Table 1. The slightly different dosages between equivalent (pumpable, self-compacting) mixes are due to the differences between the components of both batches (binder, fibers, aggregates …), in all cases aiming for the target workability.

The pumpable-type mixtures (IP, IVP, IIIP-M) achieved an S4 consistency slump class in the Abrams cone test and when poured into the formworks, these pumpable mixtures showed acceptable flowability, that required some vibration of the concrete. Some of the self-compacting mixtures (ISC, IVSC, IISC, IISC-M and IISC-Y) achieved a SF2 slump class, with a spread that was wider than 660 mm, although the presence of fibers decreased the flowability of the fresh concrete. Mixes IISC-M and IISC-Y were categorized as class SF1.

3. Properties of hardened mixtures

The mechanical characteristics in terms of strength and stiffness of the hardened mixtures are presented in Table 2. The results were from tests on 100 × 200 mm cylindrical samples conserved over one year in a moist room (20 °C and at 98% relative humidity). The dry densities of the concrete, shown in Table 2, varied between 2.52 and 2.71 Mg/m^3.

The evolution of concrete compressive strength is also shown in Table 2. At early ages (until 28 days), the mixtures can be divided into two classes by their type of cement; mixes manufactured with cement types III and IV with high volumes of pozzolanic materials (70% GGBS, 50% FA) reached strengths of around 30 MPa, while the mixes manufactured with cement types I and II reached around 50 MPa, both after 28 days in a moist room. The direct tensile strength of the samples, after 180 days in a moist room, measured with

Table 1
Mix proportions in kg per cubic meter of concrete.

	Batch 1				Batch 2		
Components in kg	IP	IVP	ISC	IVSC	IISC	IISC-M/S	IIIP-M
Cement I 52.5R	330		330				
Cement IV/B–V 32.5 N		320		320			
Cement II/B–S 42.5R					330	330	
Cement III/B 32.5 N							320
Water	160	160	170	170	170	180/185	160
EAFS medium (4–12 mm)	980	980	770	770	750	750	930
EAFS fine (0–4 mm)	690	690	550	550	550	550	690
Limestone fines (<1.18 mm)	650	650	900	900	950	950	650
Admixture (% cement weight)	1.5%	1.5%	2%	2%	1.6%	1.6%	1.4%
Fiber reinforcement (type/kg)						M/40-Y/4.5	M/38
Total weight	2815	2805	2725	2715	2700	2740/2705 (*)	2780

Roman numerals I, II, III, IV refer to the type of Portland cement as per EN-197-1. P=Pumpable; SC=Self-compacting. M = Metallic fibers; S=Synthetic fibers.
(*) = the proportioning of these two mixes in the Table amounts to 1030 L.

Table 2
Hardened properties of the mixes.

Batch	Mixture	Dry density (Mg/m^3)	E (GPa) after 90 days	ν - Poisson ratio	Compressive strength after 7-28-90-180-360 days in a moist room (MPa)	Direct tensile strength (MPa) after 180 days
1	IP	2.71	38.6	0.23	42-53-63-64-64	3.91
	IVP	2.62	31.4	0.22	18-29-36-48-56	2.83
	ISC	2.60	39.9	0.22	42-53-66-76-77	4.19
	IVSC	2.52	33.8	0.21	19-31-37-55-62	3.69
2	IISC	2.63	40.2	0.23	47-59-75-76-78	4.25
	IISC-M	2.57	34.7	0.22	38-53-63-65-69	3.77
	IISC-Y	2.54	31.6	0.22	33-46-57-59-61	3.66
	IIIP-M	2.65	26.1	0.19	20-27-33-38-42	3.14

the dog bone test (a tensile test used on rocks and high-strength concrete) [59], showed a fairly good tensility in the range of 2.5–4.5 MPa. In theory, according to the Mohr's circle applied to a single tensile test and the Tresca criterion, the shear strength should be $\tau_{max} = \sigma_{max}/2$. Fig. 1c shows a classic parabola-rectangle diagram that models the compressive strength of the sample.

The Young's modulus and the Poisson's ratio of the cylindrical samples, cured for 90 days in a moist room, yielded the elasticity parameters of the mixtures. The samples containing cement types I and II had a lineal elastic modulus in the range of 35–40 GPa and those containing cement types III and IV had a lineal elastic modulus in the range of 26–34 GPa, as shown in Table 2. In contrast the Poisson's ratio of 0.22 units was remarkably consistent, in almost all cases.

4. Shear strength testing

4.1. Specimen details and test setup

In the experimental campaign, a set of eight beams were cast for shear testing, each beam representing one of the eight mixes. The nominal beam dimension was 200 × 300 × 4400 mm, as depicted in Fig. 1, and the weight of the beam was ±0.7 Tons. The different batches of concrete beams had two different types of reinforcements: in both batches, similar 2Ø25 longitudinal reinforcement bars in the lowest positions; "light" transversal reinforcements (stirrups, see Table 3) in batch 1 (close to the "minimum design shear stress" specified in the standards), and, in batch 2, an amount of transversal reinforcement commonly found in structural RC beams.

All the beams from batches 1 and 2 were stored in the testing shed after extraction from the formwork. Batch 1 beams underwent moderate flexural loading (*i.e.* in the long-term deflection test under sustained loading, at the center of its 4.4 m span), followed by the shear-forcing loading tests on a lateral region of the beams. Consequently, these beams developed "moderate tensile cracking" (vertical cracking, smaller than one half the depth of the beam) in the tensile force test region.

A three-point bending test was chosen to evaluate the shear strength of the beams as an easier and more realistic solution than the cantilever test, which may also be applied for the same purpose, although it leads to strong reinforcement in the upper region of the beams, and complicates the application of the strut-tie model.

The shear strength of each beam was tested under three-point loading, as detailed in Fig. 2. The four beams of batch 1 had a clear span of 1600 mm between their two lower supports. The span for the batch 2 beams was reduced to 1300 mm, due to the stronger transversal reinforcements with a higher ultimate shear loading strength. Both the loading and support plates were of the same width as the beam, 200 mm. A hydraulic system of controlled displacement (0.05 mm per second) and a stiff load frame were used to perform the test, in which the foreseeable maximum loads never exceeded 50 Tons. The test lay-out is shown in Fig. 3.

Three LVDTs and 19 strain gauges were used to measure the deflection and any other deformations on the beam surfaces, as shown in Fig. 2. The high number of 19 strain gauges were firstly to detect the neutral axis (both sides, numbered 1 to 8), and secondly the appearance of eventual cracks (front side, numbered 9 to 19). Most of the data collected by the last ten strain gauges on the "front side" were of little or no significance. One datum per second was recorded during the test and the recorded variables were time, temperature, load cell measurement, three LVDT deflection displacements, and 19 strain gauge measurements. Two additional comparator clocks on the upper face of the beam (clock 1 and clock 2, see Fig. 2) were positioned on the vertical line above the supports, for visual readings and to evaluate the settlement of the support system located on the lower face of beam.

4.2. Experimental test results

After the shear-force tests, the acting load of the frame versus LVDT 2 displacement of the different specimens were plotted on the graph shown in Fig. 4. A similar behavior was observed in all the specimens under loading (in both batches). The first straight line segment describes a common linear elastic behavior up until around 104–184 kN, a segment at which the slope reflected the stiffness of

Table 3
Reinforcement characteristics.

Batch	Beams	Reinforcement			Reinforcement ratio in percentage			Span-to-depth ratio
		Top	Bottom	Stirrups	Top	Bottom	Stirrups	
1	Mix types I and IV	2Ø8	2Ø25	Ø6/200 mm	0.185	1.82	0.141	6
2	Mix types II and III	2Ø8	2Ø25	Ø8/150 mm	0.185	1.82	0.333	5

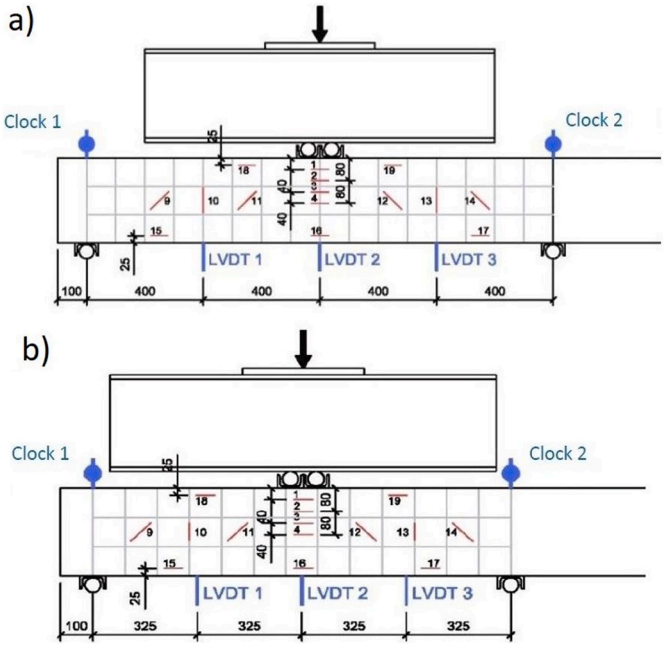

Fig. 2. Shear test setup for beams: a) Batch 1 beams; b) Batch 2 beams.

Fig. 3. Lay-out of the shear test.

the system (measurable in terms of kN/mm; the inverse of beam compliance) prior to the appearance of diagonal 45° cracking. Secondly, following a slight angular point, the curve describes a second quasi-straight segment with a gentler slope, until load values of about 200 kN in batch 1 and about 350 kN in batch 2 were reached. Thirdly, a final curved segment with a decreasing slope plots the external load forces up until the beam failure moment at the point of maximum in load, immediately before the downward slope of the curve.

The angular point precedes a decrease in the slope on the graph and corresponds to the appearance of severe 45° shear cracking in the concrete. Similar curves reported in another study [48] also reflected the same pattern (slope loss, diagonal cracking). This point reflected the moment at which the concrete failed due to a shear-force mechanism, the overall stiffness of the beam decreased, and tensile loading was transferred to the stirrups that formed part of the "steel reinforcement cage". After that angular point, a second elastic linear segment is plotted, corresponding to the linear elasticity of both the stretched steel and the compressed concrete, where the strut-tie theory could be applied.

In Fig. 5, the data from strain gauges 1 to 8 are presented, to show the bending states of the central sections of the beams throughout

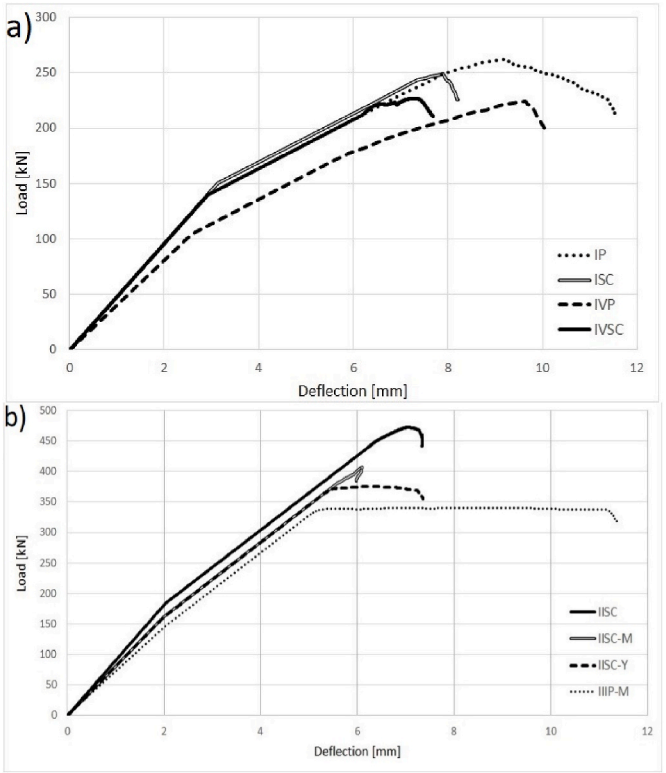

Fig. 4. Load versus deflection at mid span: a) Batch 1 beams; b) Batch 2 beams.

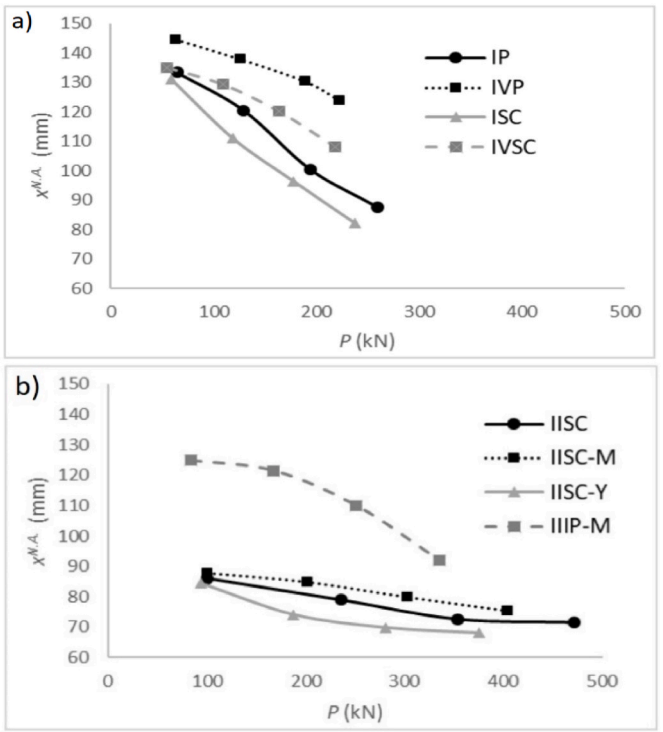

Fig. 5. Position (deep) of the neutral axis throughout the beam tests: a) Batch 1 beams; b) Batch 2 beams.

the test, and the (deep) position of the neutral axis, $X^{N.A.}$. The trends of each batch were in all cases descendent, corresponding to higher positions of the neutral axis as the load increased. The flexural moment at the center of the beam was undoubtedly increasing in the test, and the progressive bending effect produced the classic raising of the neutral axis in three-point flexural tests when the upper center of the concrete region plasticized. The difference between batches corresponded to their different clear spans. The singular behavior of both the IV-P beam in batch 1 and the IIIP-M in batch 2 may be also noted and some comments on these beams will be added in the following sections. The data from these gauges (1–8) are used to estimate the strain of both the concrete and the steel longitudinal reinforcement in the central region of the beams at any point in the test.

4.3. Shear strength of beams

Failure images of one representative specimen from each of the two batches of beams are shown in Fig. 6, reflecting the influence of each transversal reinforcement ratio. In the batch 1 of beams with a lower ratio, there were smaller loads at each significative step of the test than in the other batch. Furthermore, in batch 1, see Fig. 6a, the 45° crack opening was notable (in the order of 10 mm) and implied widespread yielding of the stirrups when the external load was close to the maximum failure value. It is worth mentioning that the form of the 45°-cracks from the lower region of the beam underwent a high degree of alteration, signaling an important role of the longitudinal reinforcement on the shear strength of the beams [60,61].

On the other hand, in the batch 2 beams with a high transversal reinforcement ratio, see Fig. 6b, the 45° shear cracks (highlighted in color) showed (about one half of a millimeter) smaller openings than in the batch 1 beams close to the ultimate load, and any yielding of stirrups, if present, was fairly reduced.

The results of the crack inclinations shown in Fig. 6b), detail clear interactions between bending moment and shear strength. The cracks propagated in an almost vertical direction at the bottom of the beam, tending towards 45° at the center-height of the beam. In the upper-top region, the angle diminished to around 30°, due to the interaction of shear stresses with compressive chord capacity of bending, producing a variable strut inclination [61,62].

As the loading of the batch 1 beams (Fig. 4a) rose to 225–260 kN, the second segment of elastic linearity reached an inflection zone, followed by a downward sloping curve. It plots the approach to the point of maximum loading in this last phase of the test, up until their failure. As the stirrups started to yield, some of the 45° cracks widened and propagated across the thickness of the whole beam from one side to the other, as can be observed from Fig. 6a. In Fig. 7, the maximum strain on the top concrete cover and the lower longitudinal steel reinforcement at the failure moment are displayed. The final failure of all four batch 1 beams was due to concrete collapse within the strongly compressed uppermost region under the external loading directly applied to each beam (rhombic points, Fig. 7, see specificity of IVP beam point); the longitudinal reinforcement also reached the yield point (square points, Fig. 7) the strain

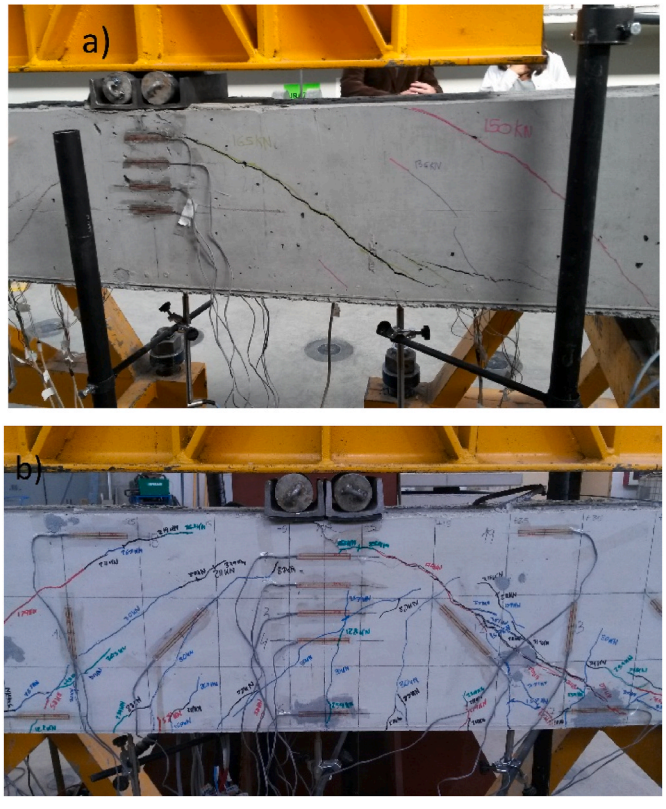

Fig. 6. The crack patterns at failure of the two batches: a) IVP (Batch 1) beam; b) IISC-Y (Batch 2) beam.

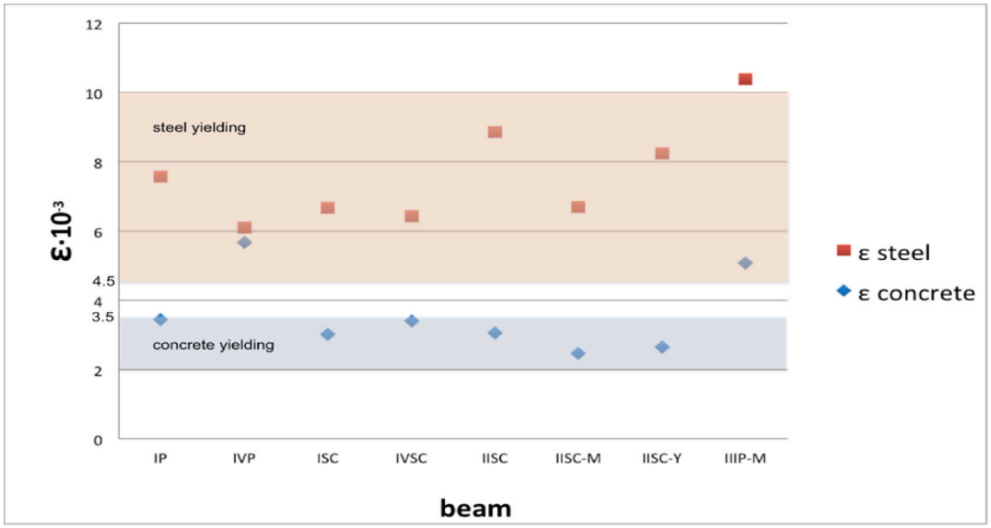

Fig. 7. Maximum material strain at the moment of beam failure.

values of which were slightly higher than the theoretical yield value 0.45%.

The second straight segment of linear elasticity after the angular point (the change from a steeper to a gentler slope) in batch 2 is visible in Fig. 4b. It extends upwards to its inflection point and the line then curves downwards towards the failure moment (340–470 kN, maximum value in the applied load). In general, the stirrups in the batch 2 beams hardly yielded (Fig. 6b) in this final zone of the curves, and the general failure was due to concrete plastic deformation in the region of the beam under strong compressive loading and subsequent collapse. Simultaneously, see Fig. 7, the longitudinal reinforcement had also begun to yield around the maximum loading and within the descending stretch of the curve reached values between 0.7 and 0.9%, though the opening of the correspondent flexural cracks was restrained; the value of 1.2% in steel strain of the IIIP-M beam deserves additional comments.

The wide yielding of the longitudinal 2Ø25 reinforcement bars in the IIIP-M beam from batch 2 is plotted as a prolonged horizontal segment in Fig. 4b. A vertical crack that had opened on the underside of the beam was detected by gauge 16 below the vertical plane of the external load. In Fig. 7, the strain value of the steel at the point of failure in this beam exceeded the theoretical steel failure value (1%); additionally, in Fig. 7, the maximum strain of the concrete largely exceeded the usual limit value of 3.5 thousand, also evidencing a singular collapse, although not so different from the other beams. A shorter horizontal segment towards the end of the IISC-Y curve also denotes noticeable, but more limited, yielding of the 2Ø25 reinforcement bars prior to compressed concrete failure.

4.4. Shear analysis

The generalized 45° cracking in the beams started at the angular point of the linear elastic field of curves in Fig. 4 (shear limit load, V_{cr}) for all the specimens. This cracking propagated widely along the second straight segment of the lineal elastic field of curves (lower slope) between V_{cr} and the ultimate strength at the maximum ordinate, V_{test}. The arithmetic difference between V_{test} and V_{cr} (the reserve shear strength), and the strength factor (ratio V_{test}/V_{cr}) are also shown in Table 4. The reserve shear strength of the batch 2 beams was generally higher than in the batch 1 beams. In practical terms, a properly designed structural element must throughout its service life support a loading shear state that is lower than the value of V_{cr} accompanying a null or very slight 45° cracking. Remember that the shear load on these beams is one half of the global vertical load applied at the center of the span (ordinates of Fig. 4), and equivalent to the reaction force in each support.

In general, the shear strength (73–92 kN) of the second batch in terms of V_{cr} was higher (±25%), than the first batch (52–75 kN), which was probably due to a higher transversal reinforcement ratio, linked to the use of the fibers. It can be stated that the suitable shear reinforcement in batch 2 beams implied a "reasonable" gain in the V_{cr} with respect the batch 1 beams.

Table 4
Shear load in the first diagonal crack and reserve shear strength.

Batch	Specimen	V_{cr} (kN)	τ_{cr} (MPa)	V_{test} (kN)	V_{test} - V_{cr} (kN)	V_{test}/V_{cr}
1	IP	70	1.58	131	61	1.87
	IVP	52	1.17	112	60	2.15
	ISC	75	1.69	126	51	1.68
	IVSC	70	1.58	113	43	1.61
2	IISC	92	2.07	235	120	2.55
	IISC-M	88	1.98	202	147	2.29
	IISC-Y	80	1.8	188	103	2.21
	IIIP-M	73	1.64	170	95	2.33

However, the ultimate failure strength (V_{test}) in batch 2 (170–235 kN) was remarkably higher (around 65%) than in batch 1 (112–131 kN). The aforementioned stronger shear reinforcement could be an insufficient justification to that noteworthy increase; probably other concurrent circumstances enhance the gain from 25% to 65%. Adding that situation to the results on the neutral axis deep of batch 1 beams, displayed in Fig. 5a, in the opinion of authors a phenomenon of softening has also taken place in the concrete mixtures of batch 1, due to its previous "historic" of loading in delayed deflection tests [33].

Two mixtures, IVP and IIIP-M, deserve comment, as they are exceptions to the generally similar concrete quality levels of each batch. Considering only the results in batch 1, the V_{cr} of the IVP mix might suggest a lower-quality concrete, but the ultimate strength, V_{test}, mainly (but not exclusively) determined by the reinforcement cage, hardly differed. Turning to the results of the IIIP-M specimen from the batch 2 beams, the unavoidable effects of the low concrete compressive strength was somewhat restored, in terms of the V_{cr} and likewise in the V_{test}, by the presence of metallic fibers. In this last beam, the final failure by tensile yielding of the lower bars hardly affected its reserve shear-strength values, shown in Table 4.

Finally, the slight yet positive influence of the metallic fibers that were added to the IISC-M and the IIIP-M mixes was not immediately obvious from an analysis of results, in view of the differing qualities of each concrete; nevertheless, their effects may be intuitively perceived from a comparison of the results of all the batch 2 beams. In the IISC-Y beam, the elastic modulus of the polymeric fibers, ten times lower than the elastic modulus of concrete, yielded an almost negligible influence.

4.5. Strut-tie model considerations

The first linear elastic segment, *i.e.* the first straight segment in Fig. 4, plots the shear forces that are simultaneously supported by both the concrete and the steel reinforcements. Their similar strain values yielded shear stress ratios for both the steel and the concrete that were equal to the elastic modulus quotient, $E_{steel}/E_{concrete}$, by the order of six units. Hence, a rough calculation of the shear stresses acting upon the angular point of the curves will be equal to the shear load (in Table 4, V_{cr}) divided by the area of the resistant section. It could be roughly evaluated as the sum of the concrete section included within the reinforcement (240 × 160 mm, excluding its cover layer) and six times (elastic modulus ratio) the steel section (1000 mm^2 from 2Ø25, overlooking the effects of the smaller bars), in total $240 \times 160 + 6000 = 44400\ mm^2$. Taking an average value of 80 kN for V_{cr} from Table 4, the resultant shear strength will be $\tau = 80000/44400 = 1.8$ MPa (see detailed values in fourth column of Table 4) which constitutes a reasonable value, considering that it should be equivalent to half of the direct tensile strength values of the mixtures in the seventh column of Table 2, according to the Tresca criterion of rupture in a Mohr's circle of uniaxial tension. The shear stress on the 2Ø25 steel bars was low (6 × 1.8 MPa = 11 MPa) up until that moment.

It is worth mentioning the experimental values of τ_{cr} detailed in Table 4 and their relationship with the results of the direct tensile tests in Table 2, the ratios of which were reasonably close to the theoretical value of σ/2 in the batch 2 mixtures. The presence of fibers was a factor that can slightly modify this equivalence. The critical shear stress values of the batch 1 mixtures were between 20 and 25% lower than the aforementioned theoretical value of σ/2; this result may be explained by the lower stiffness of the reinforcement cage (lower constraint) in batch 1, as opposed to the more robust reinforcement cage of the batch 2 beams, a key constraint factor in the shear strength of the concretes according to the Mohr circle theory.

Strut-tie modelling [63] could be reasonably applied at the initiation of wide diagonal cracking in the concrete (fissures at ±45°, V_{cr} load), at the angular inflection on the graph. The 45°-struts of concrete were withstanding compressive force ($\pm 80 \cdot \sqrt{2} = 110$ kN) and the vertical steel stirrup ties (in partial collaboration with the shear force fraction supported by the longitudinal 2Ø25 reinforcement bars) were withstanding the tensile stress of 80 kN. The compressive stress within the concrete struts was small (dividing the 110 kN load by a representative section of 100 mm thick struts, multiplied by a beam width of 200 mm yields an average stress of around 5 MPa). However, the stress on the (stirrup steel) tie was high. Logically, the propagation of the 45° concrete cracks must have redistributed the compressive and shear forces, changing the apparent compliance of the beams.

The redistribution of forces is reflected by the second straight segment, within the linear elastic field of the (steel, concrete) materials. Consequently, in Fig. 4, the second straight segment plots a gentler slope than the first segment, as the 45° cracked concrete is unable to contribute to support forces. In fact, for batch 1, the average initial slopes of the first and second segments amounted to 45 kN/mm and close to 22 kN/mm, respectively. In batch 2, the corresponding values were 80 kN/mm, and 55–60 kN/mm, respectively. The different clear spans of each batch led to differing deflection and slope values, in cubic proportion.

The forces acting along the second straight segments of the graph were analyzed, using the same rough calculations. The efficient section of stirrups was Ø6/200 mm (equivalent to 56 mm^2 every 200 mm) in batch 1 and Ø8/150 mm (equivalent to 100 mm^2 every 150 mm) in batch 2. Their load capacities were 28 and 50 kN, respectively, with the usual steel qualities.

Considering the data in Table 4, the shear force in batch 1 amounted to 131 kN at the moment of beam failure, V_{test}. As can be observed for batch 1, in Fig. 6a, each well-developed 45° crack was sewn by two stirrups, which had a total strength of 2 × 28 = 56 kN. As the stirrups yielded, the mouth of the cracks opened, and the lowermost longitudinal bars absorbed the remainder of the shear forces up until 131 kN, *i.e.* 75 kN. The moment of final collapse in this batch occurred under concrete plasticity, which is especially evident in the IVP beam, as shown in Fig. 7.

In Table 4 and in Fig. 6b likewise, the shear force is shown for batch 2, amounting to 235 kN. Each crack was "sewn" by three stirrups the total strength of which amounted to 3 × 50 = 150 kN. The 45° cracks never fully opened, so the stirrups hardly reached their yield point. The rest of the shear force, 235-150 kN = 85 kN, was absorbed by the longitudinal bars, and the final collapse was under the same concrete plasticity levels of the preceding batch, especially evident in IIIP-M beam, see Fig. 7.

4.6. Theoretical calculations of beam shear strength based on current standards and other recent theories

Some estimates of beam shear strength were performed for comparisons with the subsequent experimental results, so as to verify

which of the medium-strength EAFS aggregate concretes were acceptable for ordinary constructive applications. The predictions were performed using the specifications from the following standards: Spanish EHE-08 code section 44.2 [64], ACI318-19 chapter 22.5 [65], Model Code MC2010 section 7.3.3 level III [66,67], and the resources of the American Association of State Highway and Transportation Officials (AASHTO). Additionally, some recent analytical approaches from the bibliography were used: RESPONSE [68] software, based on the modified compression field theory (MFCT) [69], and the analytical approach proposed by Marí et al. [61,62,70–72].

The results are shown in Table 5. The calculations took account of the results of the mechanical tests on concrete mixes, presented in Table 2, and a strut inclination of 45°, acceptable in ordinary structural beams. The predictions with the formulas from the above-mentioned standards and the theoretical approach of Marí et al. were computed using concrete strengths at 28 days; concrete strength at 90 days, considered a more realistic value, was used to calculate the predictions with the MCFT method.

In Table 6, the experimental ultimate shear strengths of all the mixtures are represented as the $V_{test}/V_{predicted}$ ratio calculated with the above-mentioned standards and analytical approaches. In Fig. 8, the same ratios between the experimental and the predicted strengths are depicted.

These results can be grouped into two sets. On the one hand, the results of the structural concrete design calculations from the selected standards (Spanish EHE, ACI code, MC2010, code and AASTHO code). On other hand, the results of the experimental calculations used to verify the real condition of the structures designed and built in the past, from both the Marí and the MCFT methods. Logically, higher values than the unit may be expected in the first case (four numerical columns of Table 6), while the ratios from the "verification systems" should surround the unit (two following columns in Table 6).

In general, AASTHO proved to be the most conservative, while the ACI standard was less so: with values over 1.44 and 1.25 units, respectively. In both cases, the scatter of the results for the eight beams was reduced and their consistency with the experimental results was remarkable. The results of the European standard MC2010 using level III may be highlighted. It yielded visible differences between the beams from both batches; the results for batch 1 and for batch 2 were mostly lower than 1.3 units and mostly higher than 1.4 units, respectively, as shown in Fig. 8. In all, the results given by the usual calculation codes can be considered as correct, with suitable safety margins in the field of structural concrete between 25 and 45% units; a safety margin of under 20% might be seen as risky in this field.

Concerning the two verification methods, Marí and MCFT, most of the results are included in the interval 0.9–1 units. The Marí method is fairly precise with an average of 0.98 and a scattering of 0.024, as shown in Table 6. The beams, both with and without fibers, reached slightly lower failure loads than predicted by both systems. The MCFT system showed greater scattering in the case of the IP and the IIIP-M mixtures.

4.7. Final comments

The more reliable practical use of these beams in structural applications under shear forces led us to the conclusion that 45° diagonal cracking is undesirable for esthetic and durability-related reasons. In verification of this condition, the total load on the supports, given by the value V_{cr}, as defined in section 4.4, is displayed for each beam in Table 4.

Analyzing, as an example, the IISC beam, $V_{cr} = 92$ kN, the maximum load at center span must be fixed at 184 kN. Any additional flexural calculation will depend on the span, in this case 4 m, with the flexural moment at PL/4, *i.e.* 184 m kN. A coarse estimation of central section flexural capacity could be $M = 0.8\,d\,A{\cdot}fyd = 0.8{\cdot}0.26{\cdot}981{\cdot}525{\cdot}10^{-3} = 107$ m kN. Obviously, the limitation coming from the flexural moment correspond to a smaller load, P = 107 kN, and diagonal shear cracking will not appear at any moment. It is only if the span is reduced to $4 \cdot (107/187) = 2.3$ m that diagonal cracking will appear simultaneously to flexural exhaustion, with a ratio span-height in the order of $2.3/0.27 = 8.5$ units. In practice, that ratio is largely higher than this value.

5. Conclusions

Eight different concrete mixes containing EAFS as the main aggregate have been manufactured. Their main characteristics were good properties both in the fresh (pumpable and self-compacting mixes) and the hardened state. Two batches of RC beams with differing quantities of (low, medium) transversal reinforcements were prepared. Eight beams that had previously been cast and aged were loaded until failure under shear forces in real-scale mechanical tests. The main conclusions were as follows.

- The actual shear strength of the beams was generally satisfactory, and the use of EAFS aggregate was a favorable factor in that assessment. The inclusion of GGBS as an addition to cement is not a detrimental factor in the mechanical behavior of elements.

Table 5
Shear strength predictions from relevant standards and analytical approaches (kN).

BEAM	EHE08	ACI318-19	MC2010	AASTHO	MARI	MCFT
IP	102.1	104.8	99.8	90.4	140.2	124.6
IVP	89.8	87.4	86.7	75.8	113.9	116.9
ISC	102.1	104.8	102.7	90.4	140.2	128.5
IVSC	91.0	89.1	88.7	77.2	116.4	121.8
IISC	151.7	160.8	134.8	140.6	205.1	210.1
IISC-M	149.2	157.1	134.2	137.5	199.4	206.7
IISC-Y	146.1	152.6	130.8	133.7	192.4	201.5
IIIP-M	135.6	138.1	122.2	121.5	168.6	195.6

Table 6
$V_{test}/V_{predicted}$ ratio.

BEAM	EHE08	ACI318-19	MC2010	AASTHO	MARI	MCFT	P_{max} test (kN)
IP	1.29	1.26	1.32	1.46	0.94	1.06	262
IVP	1.25	1.28	1.29	1.48	0.98	0.96	224
ISC	1.22	1.25	1.26	1.44	0.96	0.91	252
IVSC	1.22	1.25	1.26	1.44	0.96	0.91	226
IISC	1.36	1.28	1.53	1.47	1.01	0.98	470
IISC-M	1.29	1.23	1.44	1.40	0.97	0.93	404
IISC-Y	1.31	1.26	1.47	1.43	1.00	0.95	376
IIIP-M	1.25	1.23	1.39	1.40	1.01	0.87	340
Mean (μ)	1.274	1.255	1.370	1.440	0.979	0.946	–
S.D. (σ)	0.045	0.018	0.096	0.027	0.024	0.053	–

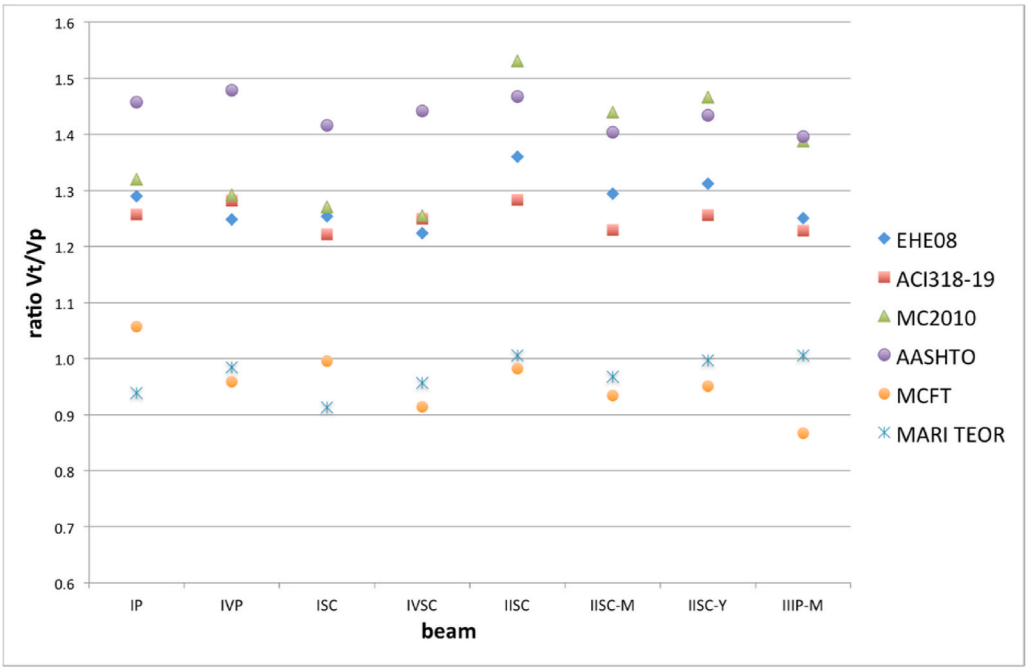

Fig. 8. Vtest/Vpredicted ratio by standard and analytical approaches.

- The results of the shear-force tests, in terms of load versus deflection curves, showed two main regions corresponding to the states before and after the development of typical shear cracking at an angle close to 45°.
- The reinforcement cage of the concrete is an important factor in its shear strength. Its stiffness (mainly due to the stiffness of the transversal reinforcements or stirrups) was a crucial variable in withstanding shear forces and in their high ultimate strength.
- The experimental shear strengths of the structural elements were consistent with strut-tie modelling and with the results of the mechanical tensile tests previously performed on the hardened concrete mixtures.
- The presence of metallic fiber reinforcement in some beams of the second batch was a favorable factor contributing to the shear strength of the structural elements, despite the workability loss of fresh concrete. The polymeric fiber additions had less visible effects on the mechanical shear strength.
- The shear strength predictions obtained with a wide range of design standards were conservative, indicating high quality structural components. Some other analytical tests on the real beams also yielded reasonable agreement with the experimental results, although in some cases the results were rather less than conservative.

Author statement

Amaia Santamaria: conceptualization, methodology, experimentation. **Jesús María Romera**: formal analysis, validation. **Ignacio Marcos**: methodology, data curation, writing-review & editing. **Víctor Revilla-Cuesta**: data curation, investigation, experimentation. **Vanesa Ortega-López**: resources, writing-review & editing, supervision, project administration, funding acquisition.

Declaration of competing interest

The authors declare that they have no known competing financial interests or personal relationships that could have appeared to influence the work reported in this paper.

Acknowledgements

This work was supported by the Spanish Ministry of Universities, MICINN, AEI, EU and ERDF [PID2020-113837RB-I00; RTI2018-097079-B-C31; 10.13039/501100011033; FPU17/03374]; the Junta de Castilla y León and ERDF [UIC-231, BU119P17]; Youth Employment Initiative (JCyL) and ESF [UBU05B_1274]; the University of Burgos [grant number SUCONS, Y135.GI], and, finally, our thanks also go to the SAREN research group (IT1619-22, Basque Government) and likewise to CHRYSO and HORMOR for supplying the materials for research.

References

[1] I.Z. Yildirim, M. Prezzi, Use of Steel Slag in Subgrade Applications, Joint Transportation Research Program, Indiana Department of Transportation and Purdue University, West Lafayette, Indiana: Publication FWA/IN/JTRP-2009/322009.
[2] B. Fronek, P. Bosela, N. Delatte, Steel slag aggregate used in portland cement concrete, Transport. Res. Rec. (2012) 37–42, https://doi.org/10.3141/2267-06.
[3] A.S. Brand, J.R. Roesler, Steel furnace slag aggregate expansion and hardened concrete properties, Cement Concr. Compos. 60 (2015) 1–9, https://doi.org/10.1016/j.cemconcomp.2015.04.006.
[4] A. Santamaria, F. Faleschini, G. Giacomello, K. Brunelli, J.T. San José, C. Pellegrino, M. Pasetto, Dimensional stability of electric arc furnace slag in civil engineering applications, J. Clean. Prod. 205 (2018) 599–609, https://doi.org/10.1016/j.jclepro.2018.09.122.
[5] A. Liapis, E.K. Anastasiou, M. Papachristoforou, I. Papayianni, Feasibility study and criteria for EAF slag utilization in concrete products, J. Sust. Metal. 4 (1) (2018) 68–76, https://doi.org/10.1007/s40831-017-0152-2.
[6] K. Morino, E. Iwatsuki, Utilization of Electric Arc furnace oxidizing slag, in: Proceedings of global symposium on recycling, waste treatment and clean technology (REWAS 1999), San Sebastián, Spain, 1999, pp. 521–530.
[7] S. Roy, T. Miura, H. Nakamura, Y. Yamamoto, Investigation on applicability of spherical shaped EAF slag fine aggregate in pavement concrete – fundamental and durability properties, Constr. Build. Mater 192 (2018) 555–568, https://doi.org/10.1016/j.conbuildmat.2018.10.157.
[8] M. Skaf, J.M. Manso, Á. Aragón, J.A. Fuente-Alonso, V. Ortega-López, EAF slag in asphalt mixes: a brief review of its possible re-use, Resour, Conserv. Recycl. 120 (2017) 176–185, https://doi.org/10.1016/j.resconrec.2016.12.009.
[9] M. Pasetto, N. Baldo, Mix design and performance analysis of asphalt concretes with electric arc furnace slag, Construct. Build. Mater. 25 (8) (2011) 3458–3468, https://doi.org/10.1016/j.conbuildmat.2011.03.037.
[10] F. Faleschini, M.A. Zanini, C. Pellegrino, New perspectives in the use of electric arc furnace slag as coarse aggregate for structural concrete, in: Proceedings of EUROSLAG 2015, Linz, 2015. Austria.
[11] I.Z. Yildirim, M. Prezzi, Chemical, mineralogical, and morphological properties of steel slag, Adv. Civ. Eng. (2011) 463638, https://doi.org/10.1155/2011/463638.
[12] F. Fiol, C. Thomas, C. Muñoz, V. Ortega-López, J.M. Manso, The influence of recycled aggregates from precast elements on the mechanical properties of structural self-compacting concrete, Constr. Build. Mater. 182 (2018) 309–323, https://doi.org/10.1016/j.conbuildmat.2018.06.132.
[13] A.S. Brand, J.R. Roesler, Interfacial transition zone of cement composites with steel furnace slag aggregates, Cement Concr. Compos. 86 (2018) 117–129, https://doi.org/10.1016/j.cemconcomp.2017.11.012.
[14] J.M. Manso, D. Hernández, M.M. Losáñez, J.J. González, Design and elaboration of concrete mixtures using steelmaking slags, ACI Mater. J. 108 (6) (2011) 673–681.
[15] Y. Jiang, T.C. Ling, C. Shi, S.Y. Pan, Characteristics of steel slags and their use in cement and concrete—a review, Resour. Conserv. Recycl. 136 (2018) 187–197, https://doi.org/10.1016/j.resconrec.2018.04.023.
[16] M. Etxeberria, C. Pacheco, J.M. Meneses, I. Berridi, Properties of concrete using metallurgical industrial by-products as aggregates, Construct. Build. Mater. 24 (9) (2010) 1594–1600, https://doi.org/10.1016/j.conbuildmat.2010.02.034.
[17] S.I. Abu-Eishah, A.S. El-Dieb, M.S. Bedir, Performance of concrete mixtures made with electric arc furnace (EAF) steel slag aggregate produced in the Arabian Gulf region, Construct. Build. Mater. 34 (2012) 249–256, https://doi.org/10.1016/j.conbuildmat.2012.02.012.
[18] C. Pellegrino, P. Cavagnis, F. Faleschini, K. Brunelli, Properties of concretes with black/oxidizing electric arc furnace slag aggregate, Cement Concr. Compos. 37 (1) (2013) 232–240, https://doi.org/10.1016/j.cemconcomp.2012.09.001.
[19] C. Pellegrino, V. Gaddo, Mechanical and durability characteristics of concrete containing EAF slag as aggregate, Cement Concr. Compos. 31 (9) (2009) 663–671, https://doi.org/10.1016/j.cemconcomp.2009.05.006.
[20] J.A. Polanco, J.M. Manso, J. Setién, J.J. González, Strength and durability of concrete made with electric steelmaking slag, ACI Mater. J. 108 (2) (2011) 196–203.
[21] F. Faleschini, M. Alejandro Fernández-Ruíz, M.A. Zanini, K. Brunelli, C. Pellegrino, E. Hernández-Montes, High performance concrete with electric arc furnace slag as aggregate: mechanical and durability properties, Construct. Build. Mater. 101 (2015) 113–121, https://doi.org/10.1016/j.conbuildmat.2015.10.022.
[22] Y. Wang, P. Suraneni, Experimental methods to determine the feasibility of steel slags as supplementary cementitious materials, Construct. Build. Mater. 204 (2019) 458–467, https://doi.org/10.1016/j.conbuildmat.2019.01.196.
[23] I.Z. Yildirim, M. Prezzi, EAF ladle steel slag as a geo-material: compaction and shear strength characteristics, in: Proceedings of IFCEE 2018: Advances in Geomaterial Modeling and Site Characterization, Orlando, Florida, USA, 113–122. https://doi.org/10.1061/9780784481585.012.
[24] H. Qasrawi, Towards sustainable self-compacting concrete: effect of recycled slag coarse aggregate on the fresh properties of SCC, Adv. Civ. Eng. 2018 (2018) 7450943, https://doi.org/10.1155/2018/7450943.
[25] A. Santamaría, A. Orbe, J.T. San José, J.J. González, A study on the durability of structural concrete incorporating electric steelmaking slags, Construct. Build. Mater. 161 (2018) 94–111, https://doi.org/10.1016/j.conbuildmat.2017.11.121.
[26] B.S. Cho, Y.C. Choi, Hydration properties of STS-refining slag-blended blast furnace slag cement, Adv. Mater. Sci. Eng. 2018 (2018) 5893254, https://doi.org/10.1155/2018/5893254.
[27] A. Santamaría, E. Rojí, M. Skaf, I. Marcos, J.J. González, The use of steelmaking slags and fly ash in structural mortars, Construct. Build. Mater. 106 (2016) 364–373, https://doi.org/10.1016/j.conbuildmat.2015.12.121.
[28] V.Z. Serjun, B. Mirtič, A. Mladenovič, Evaluation of ladle slag as a potential material for building and civil engineering, Mater. Tehnologije 47 (5) (2013) 543–550.
[29] G. Aragón, Á. Aragón, A. Santamaría, A. Esteban, F. Fiol, Physical and mechanical characterization of a commercial rendering mortar using destructive and non-destructive techniques, Construct. Build. Mater. 224 (2019) 835–849, https://doi.org/10.1016/j.conbuildmat.2019.07.034.
[30] F. Faleschini, P. De Marzi, C. Pellegrino, Recycled concrete containing EAF slag: environmental assessment through LCA, Eur. J. Environ. Civ. Eng. 18 (9) (2014) 1009–1024, https://doi.org/10.1080/19648189.2014.922505.
[31] A.K. Saha, M.N.N. Khan, P.K. Sarker, Value added utilization of by-product electric furnace ferronickel slag as construction materials: a review, Resour. Conserv. Recycl. 134 (2018) 10–24, https://doi.org/10.1016/j.resconrec.2018.02.034.

[32] H. Qasrawi, The use of steel slag aggregate to enhance the mechanical properties of recycled aggregate concrete and retain the environment, Construct. Build. Mater. 54 (2014) 298–304, https://doi.org/10.1016/j.conbuildmat.2013.12.063.
[33] A. Santamaría, V. Ortega-López, M. Skaf, J.A. Chica, J.M. Manso, The study of properties and behavior of self compacting concrete containing Electric Arc Furnace Slag (EAFS) as aggregate, Ain Shams Eng. J. 11 (1) (2020) 231–243, https://doi.org/10.1016/j.asej.2019.10.001.
[34] S.W. Kim, Y.J. Lee, K.H. Kim, Flexural behavior of reinforced concrete beams with electric arc furnace slag aggregates, J. Asian Architect. Build Eng. 11 (1) (2012) 133–138, https://doi.org/10.3130/jaabe.11.133.
[35] S.W. Kim, Y.J. Lee, Y.H. Lee, K.H. Kim, Flexural performance of reinforced high-strength concrete beams with EAF oxidizing slag aggregates, J. Asian Architect. Build Eng. 15 (3) (2016) 589–596, https://doi.org/10.3130/jaabe.15.589.
[36] Y.J. Lee, H.G. Kim, J.H. Park, K.S. Lee, K.H. Kim, Flexural behaviour prediction for RC beams in consideration of compressive stress distribution of concrete with electric arc furnace oxidising slag aggregates, Eur. J. Environ. Civ. Eng. 24 (5) (2020) 689–708, https://doi.org/10.1080/19648189.2017.1417916.
[37] S.W. Kim, Y.S. Kim, J.M. Lee, K.H. Kim, Structural performance of spirally confined concrete with EAF oxidizing slag aggregate, Eur. J. Environ. Civ. Eng. 17 (8) (2013) 654–674, https://doi.org/10.1080/19648189.2013.810178.
[38] S.W. Kim, Y.J. Lee, K.H. Kim, Bond behavior of RC beams with electric arc furnace oxidizing slag aggregates, J. Asian Architect. Build Eng. 11 (2) (2012) 359–366, https://doi.org/10.3130/jaabe.11.359.
[39] C. Pellegrino, F. Faleschini, Experimental behavior of reinforced concrete beams with electric arc furnace slag as recycled aggregate, ACI Mater. J. 110 (2) (2013) 197–205.
[40] F. Faleschini, L. Hofer, M.A. Zanini, M. dalla Benetta, C. Pellegrino, Experimental behavior of beam-column joints made with EAF concrete under cyclic loading, Eng. Struct. 139 (2017) 81–95, https://doi.org/10.1016/j.engstruct.2017.02.038.
[41] F. Faleschini, A. Santamaria, M.A. Zanini, J.T. San José, C. Pellegrino, Bond between steel reinforcement bars and electric arc furnace slag concrete, Mater. Struct. 50 (3) (2017) 170, https://doi.org/10.1617/s11527-017-1038-2.
[42] P. Pujadas, A. Blanco, S.H.P. Cavalaro, A. de la Fuente, A. Aguado, Flexural post-cracking creep behaviour of macro-synthetic and steel fiber reinforced concrete, RILEM Bookseries 14 (2017) 77–87, https://doi.org/10.1007/978-94-024-1001-3_7.
[43] E. Cuenca, J. Echegaray-Oviedo, P. Serna, Influence of concrete matrix and type of fiber on the shear behavior of self-compacting fiber reinforced concrete beams, Compos. B Eng. 75 (2015) 135–147, https://doi.org/10.1016/j.compositesb.2015.01.037.
[44] N.H. Roslan, M. Ismail, N.H.A. Khalid, B. Muhammad, Properties of concrete containing electric arc furnace steel slag and steel sludge, J. Build. Eng. 28 (2020) 101060, https://doi.org/10.1016/j.jobe.2019.101060.
[45] Y.W. Choi, H.K. Lee, S.B. Chu, S.H. Cheong, W.Y. Jung, Shear behavior and performance of deep beams made with self-compacting concrete, Ind. J. Concr. Struct. Mater. 6 (2) (2012) 65–78, https://doi.org/10.1007/s40069-012-0007-y.
[46] B. González-Fonteboa, F. Martínez-Abella, Shear strength of recycled concrete beams, Construct. Build. Mater. 21 (4) (2007) 887–893, https://doi.org/10.1016/j.conbuildmat.2005.12.018.
[47] N. Tošić, S. Marinković, I. Ignjatović, A database on flexural and shear strength of reinforced recycled aggregate concrete beams and comparison to Eurocode 2 predictions, Construct. Build. Mater. 127 (2016) 932–944, https://doi.org/10.1016/j.conbuildmat.2016.10.058.
[48] I.S. Ignjatović, S.B. Marinković, N. Tošić, Shear behaviour of recycled aggregate concrete beams with and without shear reinforcement, Eng. Struct. 141 (2017) 386–401, https://doi.org/10.1016/j.engstruct.2017.03.026.
[49] B. González-Fonteboa, F. Martínez-Abella, I. Martínez-Lage, J. Eiras-López, Structural shear behaviour of recycled concrete with silica fume, Construct. Build. Mater. 23 (11) (2009) 3406–3410, https://doi.org/10.1016/j.conbuildmat.2009.06.035.
[50] K.N. Rahal, Y.T. Alrefaei, Shear strength of longitudinally reinforced recycled aggregate concrete beams, Eng. Struct. 145 (2017) 273–282, https://doi.org/10.1016/j.engstruct.2017.05.028.
[51] S.A. Waseem, B. Singh, Shear transfer strength of normal and high-strength recycled aggregate concrete – an experimental investigation, Construct. Build. Mater. 125 (2016) 29–40, https://doi.org/10.1016/j.conbuildmat.2016.08.022.
[52] H. Katkhuda, N. Shatarat, Shear behavior of reinforced concrete beams using treated recycled concrete aggregate, Construct. Build. Mater. 125 (2016) 63–71, https://doi.org/10.1016/j.conbuildmat.2016.08.034.
[53] A.E.K.S. Soliman, M.A.M. Osman, Efficiency of using discrete fibers on the shear behavior of R.C. beams, Ain Shams Eng. J. 3 (3) (2012) 209–217, https://doi.org/10.1016/j.asej.2012.03.006.
[54] CEN, European Committee for Standardization. Rue de Stassart, 36. Brussels B-1050,.
[55] Annual Book of ASTM Standards, 2008, pp. 19429–22959.
[56] A. Santamaría, A. Orbe, M.M. Losañez, M. Skaf, V. Ortega-Lopez, J.J. González, Self-compacting concrete incorporating electric arc-furnace steelmaking slag as aggregate, Mater. Des. 115 (2017) 179–193, https://doi.org/10.1016/j.matdes.2016.11.048.
[57] S. Grünewald, F. Laranjeira de Oliveira, J. Walraven, A. Aguado de Cea, C. Molins i Borrell, Influence of fibre orientation on the performance of steel fibre-reinforced concrete, in: Proceedings of Eightht RILEM International Symposium on Fibre Reinforced Concrete, BEFIB, Guimarães, Portugal, 2012, pp. 1–12.
[58] J.T. San-José, J.M. Manso, Fiber-reinforced polymer bars embedded in a resin concrete: study of both materials and their bond behavior, Polym. Compos. 27 (3) (2006) 315–322, https://doi.org/10.1002/pc.20188.
[59] Z. Zhou, P. Qiao, Direct tension test for characterization of tensile behavior of UHPC, J. Test. Eval. 48 (2020), https://doi.org/10.1520/JTE20170644.
[60] A.S. El-Dieb, T.A. El-Maaddawy, O. Al-Rawashdah, Shear behavior of ultra-high strength steel fiber-reinforced self-compacting concrete beams, in: Proceedings of the First Congress on Construction Materials and Structures, ICCMATS1, Johannesburg, South Africa, 2014, pp. 972–979, https://doi.org/10.3233/978-1-61499-466-4-972.
[61] A. Marí, J.M. Bairán, A. Cladera, E. Oller, Shear design and assessment of reinforced and prestressed concrete beams based on a mechanical model, S. Struct. Eng. 142 (10) (2016) 4016064, https://doi.org/10.1061/(ASCE)ST, 1943-541X.0001539.
[62] A. Marí, A. Cladera, J. Bairán, E. Oller, C. Ribas, Shear-flexural strength mechanical model for the design and assessment of reinforced concrete beams subjected to point or distributed loads, Front. Struct. Civ. Eng. 8 (4) (2014) 337–353, https://doi.org/10.1007/s11709-014-0081-0.
[63] E.S. Khalifa, Macro-mechanical strut and tie model for analysis of fibrous high-strength concrete corbels, Ain Shams Eng. J. 3 (4) (2012) 359–365, https://doi.org/10.1016/j.asej.2012.04.004.
[64] EHE-08, Concrete Standard/Instrucción de Hormigón Estructural, 2008.
[65] RILEM Recommendations for the Testing and Use of Constructions Materials, 1994 vols. 34–35.
[66] International Federation for Structural Concrete, Fib Model Code for Concrete Structures, 2010.
[67] V. Sigrist, E. Bentz, M.F. Ruiz, S. Foster, A. Muttoni, Background to the fib Model Code 2010 shear provisions - Part I: beams and slabs, Struct. Concr. 14 (3) (2013) 195–203, https://doi.org/10.1002/suco.201200066.
[68] M.P. Collins, D. Mitchell, Prestressed Concrete Structures, Prentice-Hall, Englewood Cliffs, N.J, 1991.
[69] F.J. Vecchio, M.P. Collins, Modified compression-field theory for reinforced concrete elements subjected to shear, J. Am. Concr. Inst. 83 (2) (1986) 219–231.
[70] A. Cladera, A.R. Marí, Shear design procedure for reinforced normal and high-strength concrete beams using artificial neural networks. Part II: beams with stirrups, Eng. Struct. 26 (7) (2004) 927–936, https://doi.org/10.1016/j.engstruct.2004.02.011.
[71] A. Marí, A. Cladera, J. Bairán, E. Oller, C. Ribas, Un modelo unificado de resistencia a flexión y cortante de vigas esbeltas de hormigón armado bajo cargas puntuales y repartidas, Hormigón y Acero 65 (2014) 247–265, https://doi.org/10.1016/j.hya.2014.11.001.
[72] A. Marí, J. Bairán, A. Cladera, E. Oller, C. Ribas, Shear-flexural strength mechanical model for the design and assessment of reinforced concrete beams, Struct. Infrastruct. Eng. 11 (11) (2015) 1399–1419, https://doi.org/10.1080/15732479.2014.964735.